

Epidemics: Models and data using R (2nd edition)

Ottar N. Bjørnstad

June 11, 2022

For Katriona, Esme and Michael

Preface

Preface to 2nd edition

As with the first edition, the second edition has further benefitted heavily from input from numerous people, particularly my various students, postdocs and collaborators. The book club at the London School of Tropical Medicine and Hygiene provided valuable feedback on the first edition clarifying how the text should be better fleshed out and organized. Reorganizing, restructuring and recoding meant that the current material is not fully back-compatible, so the `epimdr2` R package should be used with the new edition. Typesetting of equations have been changed for clarity and shinyApps have largely been reparameterized with reproduction number, R_0 , rather than transmission rate (β) since that is more intuitive. The SARS-CoV-2 pandemic spurred significant new analyses of infectious disease dynamics. Much of the new age-structured modeling in Chap. 4 were developed with Jessica Metcalf, Ruiyun Li and Dami Pak. The catalytic model is now discussed in a separate chapter (Chap. 5). New competing strain models have been added (Sect. 3.12). The chapter on networks has been greatly expanded. Functions for automation of Jacobian matrices and next generation calculation are presented. A new chapter on invasion and persistence (Chap. 15) has new treatment of zoonoses including visits on branching processes, spatial diffusion, synchrony and metapopulation persistence. New data sets were provided by Lance Waller and Laura Pomeroy as well as various publicly available sources. Rustom Antia has kindly helped me better understand the rudiments of adaptive immunity and immune memory.

To understand the philosophy behind this text I encourage any reader to peruse the preface to the first edition.¹ While the R ecosystem is evolving rapidly, I have deliberately striven to use generic S3 code for all calculations (except for occasional straying for animations etc in accompanying ShinyApps) for the reason that I didactically believe that the logic of programming with data laid out by Chambers (1998) is the simplest and most elegant way. With respect to mathematical symbols, I have

¹ The preface to the first edition has been updated so chapter and section labels are consistent with the new text.

tried as best as possible to be consistent in usage (thus some changes in notation from 1st edition) such that for example β is generally used for transmission, ϕ for force of infection, ω for loss of immunity, rates are lowercase greek and probabilities are uppercase greek, etc. The text covers a lot of material, though, so keeping the greek alphabet soup sorted has been challenging.

In addition to previous funding this text has also benefitted from support from the Norwegian Research Council. The text and associated teaching materials have been my main passion for almost a decade.

Ottar N. Bjørnstad
University Park,
May 2022

Preface to 1st edition

Despite an undergraduate degree in Zoology and a MSc on the behavior of voles, I have long been fascinated by theoretical biology and the relationship between models and data, and the feedback between statistical analysis and conceptual developments in the area of infectious disease dynamics, in particular, and ecological dynamics in general. My perpetual frustration has been to read all the wonderfully clever books and journal articles exuding all sort of nifty maths and stats, but not quite being able to *do* any of it myself when it came to infectious diseases that I care about. This frustration led me to make myself some worked examples of all this cleverness. Over the years the stack of how-to's has grown, and the following chapters are an attempt at organizing these so they may be useful to others. I have tried to organize the chapters and sections in a reasonably logical way: Chaps. 2–11 is a mix and match of models, data and statistics pertaining to local disease dynamics; Chaps. 12–15 pertains to spatial and spatiotemporal dynamics; Chap. 16 highlights similarities between the dynamics of infectious disease and parasitoid–host dynamics; Finally, Chaps. 17–18 overviews additional statistical methodology I have found useful in the study of infectious disease dynamics. Some sections are marked as “advanced” for one of two reasons: (i) either the maths or stats is a bit more involved and/or (ii) the topic in focus is a bit more esoteric. Although not marked as such, most of Chap. 11 is advanced in this respect. While less run-of-the-mill, I have thought it important to include these sections, because they cover topics that may be less easy to find code for elsewhere.

I have had invaluable help from students, colleagues and collaborators in my quest. The pre-conference workshops of “Ecology and Evolution of Infectious Disease” that I co-taught between 2005 and 2008 enhanced my motivation to annotate many worked examples; Bare-bones of several of the following sections were written during frantic 24hrs stints prior to these workshops. Much of the other material arose from interactions with students and post-docs at Pennsylvania State University’s Center for Infectious Disease Dynamics (CIDD). Parts of the epidemics on networks and the R_0 removal estimator is from Matt Ferrari’s PhD research, the age-structured SIR simulator and the SIRWS model is from Jennie Lavine’s PhD work. Working with distributed-delay models has been a collaboration with Bill Nelson and my students Lindsay Beck-Johnson and Megan Greischar. Angie Luis and I cooked up the code to do transfer functions in R as part of her PhD research. Much of the code on the catalytic model is from collaborations with Laura Pomeroy and then-CIDD postdoctoral fellows Grainne Long and Jess Metcalf. The in-host TSIR was also a collaboration with Jess. The Gillespie code arose from collaborations with postdoctoral fellow Shouli Li and my honor student Reilly Mumma. Reilly also taught me how to write my first shinyApp. Away from Penn State, Aaron King and Ben Bolker have at various times been unbelievably patient in teaching me bits of maths I didn’t understand. Roger Nisbet painstakingly guided me through my first transfer functions during my postdoctoral fellowship at NCEAS. During the same period Jordi Bascompte introduced me to coupled-map lattice models. Finally,

Bryan Grenfell showed me wavelets and introduced me to the field of infectious disease dynamics some 20 years ago.

The data used has been kindly shared by Janis Antonovics, Jeremy Burdon, Rebecca Grais, Sylvijs Huygen, Jenn Keslow, Sandy Leibhold, Grainne Long and Mary Poss. The first draft of the text was completed while I was on sabbatical at the University of Western Australia and University of Oslo / the Norwegian Veterinary Institute during 2017. My work leading up to this text has variously been funded by the National Science Foundation, the National Institute of Health, the US Department of Agriculture and the Bill and Melinda Gates Foundation.

Contents

1	Introduction	3
1.1	Preamble	3
1.2	In-Host Persistence	4
1.3	Patterns of Endemicity	6
1.4	R	8
1.5	Resources	10
 Part I Time		
2	SIR	13
2.1	Introduction	13
2.2	The SIR model	13
2.3	Numerical Integration of the SIR Model	16
2.4	Final Epidemic Size	18
2.5	The Open Epidemic	21
2.6	Phase Analysis	22
2.7	Stability and Periodicity	24
2.8	Heterogeneities	26
2.9	Advanced: More Realistic Infectious Periods	27
2.10	A SIR ShinyApp	31
3	R_0	35
3.1	Primacy of R_0	35
3.2	Rates and Probabilities	36
3.3	Estimating R_0 From a Simple Epidemic	37
3.4	The Chain-Binomial Model	39
3.5	Stochastic Simulation	44
3.6	Further Examples	45
3.7	R_0 from S(E)IR Flows	51
3.8	Other Rules of Thumb	52
3.9	Advanced: The Next-Generation Matrix	54

3.10 SEIHFR	56
3.11 A Next-Generation R_0 Function	60
3.12 A Two-Strain ShinyApp	62
4 FoI and Age-Dependence	69
4.1 Force of Infection	69
4.2 Burden of Disease	70
4.3 WAIFW	71
4.4 A RAS Model	72
4.5 Virgin Epidemics	78
4.6 Vaccination by Age-Dependent Risk.....	80
4.7 Projecting Host Age-Structure	83
5 The Catalytic Model	89
5.1 Immune Memory	89
5.2 The Catalytic Model	90
5.3 More Flexible ϕ -Functions	93
5.4 A Log-Spline Model	97
5.5 Rubella	100
6 Seasonality	107
6.1 Environmental Drivers	107
6.2 The Seasonally Forced SEIR Model	110
6.3 Seasonality in β	112
6.4 Bifurcation Analysis	115
6.5 Stroboscopic Section	116
6.6 Susceptible Recruitment	117
6.7 A Forced SEIR ShinyApp	120
6.8 A Jacobian Function	120
7 Time Series Analysis	123
7.1 Taxonomy of Methods	123
7.2 Time Domain: ACF and ARMA	123
7.3 ARMA	124
7.4 Frequency Domain	128
7.5 Time/Frequency hybrids: Wavelets	128
7.6 Measles in London	130
7.7 Project Tycho	135
7.8 Lomb Periodogram: Whooping Cough	136
7.9 Triennial Cycles: Philadelphia Measles	138
7.10 Wavelet Reconstruction and Wavelet Filter: Diphtheria	138
7.11 Advanced: FFT and Reconstruction	142

Contents	xiii
8 TSIR	145
8.1 Estimating Parameters in Dynamic Models	145
8.2 Stochastic Variability	146
8.3 Estimation Using the TSIR	148
8.4 Inference (Hypothetical)	149
8.5 Susceptible Reconstruction	150
8.6 Simulating the TSIR Model	154
8.7 Emergent Simplicity	157
8.8 Project Tycho	157
8.9 In-host Malaria Dynamics	159
8.10 A TSIR ShinyApp	163
8.11 Malapropos: A Ross-Macdonald Malaria Model	164
9 Stochastics	167
9.1 Preamble: Prevalence vs Incidence	167
9.2 Event Based Stochastic Simulation	168
9.3 Trajectory Matching	172
9.4 Likelihood Theory 101	174
9.5 SEIR with Error	177
9.6 Boarding School Flu Data	179
9.7 Measles	180
9.8 Outbreak Response Vaccination	183
9.9 An ORV ShinyApp	187
10 Stability and Resonant Periodicity	189
10.1 Preamble: Rabies	189
10.2 Linear Stability Analysis	191
10.3 Finding Equilibria	191
10.4 Evaluating the Jacobian	193
10.5 Influenza	195
10.6 Raccoon Rabies	197
10.7 Critical Host Density	201
10.8 Advanced: Transfer Functions	203
10.9 (Even More) Advanced: Transfer Functions and Delay Coordinates	209
10.10 SEIRS and TSIR ShinyApps	211
11 Exotica	213
11.1 Too Nonlinear	213
11.2 Chaos	213
11.3 Local Lyapunov Exponents	217
11.4 Coexisting Attractors	222
11.5 Repellors / Almost attractors	226
11.6 Invasion Orbits	230
11.7 Stochastic Resonance	233
11.8 Predictability: Empirical Dynamic Modelling	236

11.9 Appendix: Making a Pomp Simulator	238
--	-----

Part II Space

12 Spatial Dynamics	245
12.1 Introduction	245
12.2 Dispersal Kernels	245
12.3 <i>Filipendula</i> Rust Data	246
12.4 Simulation	251
12.5 Gypsy Moth	252
12.6 A Coupled Map Lattice SI Model	254
12.7 Making Movies	256
12.8 Covariance Functions for Spatiotemporal Data	257
12.9 Gravity Models	258
12.10 Appendix: A Spatial Gypsy Moth Model	261
13 Spatial and Spatiotemporal Patterns	267
13.1 Spatiotemporal Patterns	267
13.2 A Plant-Pathogen Case Study	267
13.3 Spatial Autocorrelation	269
13.4 Testing and Confidence Intervals	271
13.5 Mantel test	272
13.6 Correlograms	272
13.7 Nonparametric Spatial Correlation Functions	273
13.8 LISA	276
13.9 Cross-Correlations	276
13.10 Gypsy Moth	279
14 Transmission on Networks	281
14.1 Social Heterogeneities	281
14.2 S Preamble: Objects, Classes and Functions	282
14.3 Networks	285
14.4 Models of Networks	286
14.5 Epidemics on Networks	291
14.6 Epidemic Size Distribution	295
14.7 Empirical Networks	297
14.8 Vaccinating Networks	299
15 Invasion and Eradication	301
15.1 Invasion	301
15.2 Stage III Branching Processes	302
15.3 Phocine Distemper Virus	305
15.4 Rabies	308
15.5 Initial Control	312
15.6 Synchrony	313
15.7 Coupling	315

Contents	xv
15.8 A Synthesis	319
Part III Miscellany	
16 Parasitoids	325
16.1 Introduction	325
16.2 Parasitoid-Host Dynamics	325
16.3 Stability and Resonant Periodicity	330
16.4 Biological Control	332
16.5 Larch Bud Moth	333
16.6 Host-Parasitoid Metapopulation Dynamics	333
16.7 Parasitoid-Host ShinyApps	335
17 Quantifying In-Host Patterns	337
17.1 Motivation	337
17.2 Two Experiments	337
17.3 Data	338
17.4 PCA of the FIV Data	339
17.5 LDA of the FIV Data	341
17.6 MANOVA of FIV Data	345
17.7 PCA of the Mouse Malaria data	346
17.8 FDA of the Mouse Malaria Data	348
18 Non-Independent Data	351
18.1 Non-Independence	351
18.2 Spatial Dependence	351
18.3 Spatial Regression	353
18.4 Repeated Measures	356
18.5 Sibling Correlation	363
18.6 The End	365
Bibliography	367
References	367
Index	391

tion, a spatial network intervention, was used extensively to create immunological cordon sanitaires during the final years of smallpox eradication during which villages would be targeted as soon as a case was discovered (Henderson and Klepac, 2013). Cocooning—the idea of vaccinating all family members of at-risk children too young for immunization—is a social network intervention recommended to protect against whooping cough (e.g. Lavine et al., 2011).

In addition to these applications, there are multitudes of mathematical and computational studies on using social network consideration to think about vaccination strategies and vaccination deployment (Holme and Litvak, 2017). One amusing idea is “acquaintance vaccination” in the face of limited medical supply: pick random individuals in a network and ask them to identify a friend to be vaccinated. A friend of a random individual is likely to have a higher social connectivity and thus be more likely to contribute to onwards spread. A slightly less esoteric idea is to try to use social engineering of vaccine sentiments across a network. Fu et al. (2011) discussed this as “imitation dynamics”, a form of social diffusion, where positive (or negative) opinions and adoption practices may spread to help toward herd immunity for voluntary vaccine programs. Sociologist have discussed how such dynamics depends on network homophily: The extent to which individuals with similar views assort preferentially. With strong assortment, diffusion of ideas and sentiments will be weak whereas with weak assortment influencers may sway general opinions. Homophily seems to have been an important factor during the SARS-CoV-2 spread in 2020–21 in the US for which there was limited cross-talk among vaccine positive and vaccine skeptic segments of the population.

Models of networks and epidemics on networks is a vast literature, so the above should at best be considered a teaser. For example it only consider static networks without births, deaths or social reconfiguration. It does also not consider network modularity (Newman, 2006). Homophily is an obvious social process that leads to highly modular networks. The [statnet project](#) and associated [statnet package](#) have a rich set of resources for deeper explorations.

Chapter 15

Invasion and Eradication

15.1 Invasion

Pathogens invades new host niches all the time. The global invasion of the human niche by SARS-CoV-2 during the 2020–22 pandemic is the most recent example, but cross-species transmission is ubiquitous. In 2009 Influenza A/H1N1pdm09 emerged and spread globally most likely after a triple recombination of human, avian and porcine viral segments (Smith et al., 2009a). The HIV-1 pandemic started in the mid 20th century probably from bushmeat spillover of chimpanzee simian immunodeficiency virus, which itself is thought to have originated from spillovers from other primates, to go global in the 1970s (Hemelaar, 2012). Cross-species transmission is not just an issue of zoonotic spillover or anthropogenic spillback, it is equally important as spillover among animal species. Among the paramyxoviruses, Taber and Pease (1990) discusses how tissue tropism generally change more slowly than host specificity so that host switching is often more constrained by tissue similarity than host species identity. Phocine distemper virus, for example, is endemic to harp seals in the high arctic but have at least twice (in 1988 and 2002) invaded harbor seal populations of the North sea to cause catastrophic mortality (Hall et al., 2006).

Lloyd-Smith et al. (2009) provides a comprehensive classification of cross-species establishment of infectious diseases and thus invasion that recognizes three key stages:

- Stage II: Primary spillover wherein a pathogen cross the species border but with no onwards transmission in the secondary host. Human cases of old- and new-world hantaviruses, Bolivian hemorrhagic arenavirus fever and Junin arenavirus are all exemplars of this.
- Stage III: Subcritical (i.e. $R_0 < 1$) establishment result in stuttering chains of transmission. Lassa fever virus for which Iacono et al. (2015) estimated that

This chapter uses the following R packages: `scatterplot3d`, `raster`, `gdistance`, `maptools`, `rgdal`, `maps` and `ncf`.

A five minute epidemics MOOC on spatial spread can be seen on YouTube: <https://www.youtube.com/watch?v=WPjsAdyD1Gg>

about 20% of cases are human-to-human and the rest are spillover from the multimammate mouse (*Mastomys natalensis*) is a good example. So also is another rodent-borne infection, monkey pox, for which Blumberg and Lloyd-Smith (2013b) estimated a human-to-human R_0 of 0.3 that has recently risen to 0.8. Other notorious examples are the Nipha virus and avian influenzas (Lloyd-Smith et al., 2009).

- Stage IV represents supercritical ($R_0 > 1$) establishment. To refine Lloyd-Smith et al.’s (2009) classification, it may be useful to distinguish type IVa which causes epidemics with failure of long-term establishment from type IVb which causes long-term endemism in the derived host. HIV, influenza A/H1N1pdm09 and SARS-CoV-2 are examples of the latter. In humans, Ebola and yellow fever are examples of the former. On the animal-to-animal side, phocine distemper virus (PDV) in harbor seals is an interesting example where outbreaks are so violent that the pathogen burns out of susceptibles to result in IVa dynamics.¹

15.2 Stage III Branching Processes

The final epidemic size of Stage III subcritical spillover (sometimes called “cluster size”) is usually modeled as a Galton-Watson branching process (Farrington et al., 2003). The model is quite general and can flexibly accommodate within-population heterogeneities (Blumberg and Lloyd-Smith, 2013b). For illustrative purposes we may consider the simplest case of subcritical spread in a homogenous host population. With homogeneity and assuming the population is sufficiently large that susceptible depletion will not affect the stuttering chain, the offspring distribution (the number of onwards infecteds per infected) during a serial interval will follow a Poisson distribution with a mean of R_0 and the outbreak size distribution, O , will follow a Borel-Tanner distribution that depends on the initial number of infecteds, i_0 according to:

$$P(O = x|i_0) = \frac{i_0 x^{x-i_0-1} R_0^{x-i_0} e^{-xR_0}}{(x-i_0)!} \quad (15.1)$$

In addition to Stage III spillover, this model also applies to seeding of new chains from supercritical communities to communities that, through interventions, have achieved control. This was the case among areas of lockdown, partial lockdown and no interventions during the early SARS-CoV-2 pandemic.². For illustration consider the predicted outbreak size distribution from an initial i_0 of five individuals in communities with subcritical R_0 s of 0.5, 0.7 and 0.9:

```
R0 = 0.5
x = 1:50
i0 = 5
```

¹ Akin to the failure of persistence of measles in human communities below the critical community size (Bartlett, 1960b; Grenfell and Harwood, 1997, Sect. 1.3).

² Engen et al. (2021) discusses an alternative diffusion approximation approach to study this issue.

```

plot(i0 * x^(x - i0 - 1) * R0^(x - i0) *
     exp(-x * R0)/factorial(x - i0), xlab="Outbreak size",
     ylab="Probability", type="p")
R0 = 0.7
points(i0 * x^(x - i0 - 1) * R0^(x - i0) *
       exp(-x * R0)/factorial(x - i0), pch = 2)
R0 = 0.9
points(i0 * x^(x - i0 - 1) * R0^(x - i0) *
       exp(-x * R0)/factorial(x-i0), pch=3)
legend("topright", c("0.5", "0.7", "0.9"), pch = 1:3)

```

For these scenarios, some onwards transmissions are clearly happening with a cluster size mode of seven in the first scenario and 10 in the last scenario, but there is still a chance of seeing almost 20 cases in the former and 50 cases in the latter (Fig. 15.1).

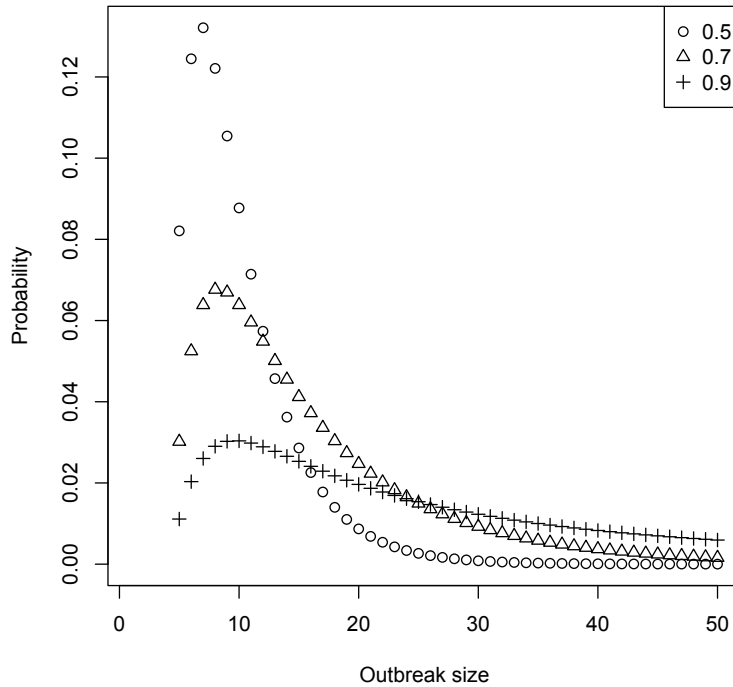


Fig. 15.1: Final epidemic size distributions predicted from the Galton-Watson branching process assuming a Poisson distributed offspring distribution and subcritical spread with R_0 s of 0.5, 0.7 and 0.9

Farrington and Grant (1999) used the branching process model to also study the distribution of lengths of stuttering chains. With the Poisson offspring distribution and a single introduction they derived that the probability that the chain will be shorter-or-equal to k generations (i.e. serial intervals) is:

$$f_k = P(G \leq k) \sim e^{-R_0} E_k(e^{R_0 e^{-R_0}}), \quad (15.2)$$

where $E_k(x)$ is the “iterated exponential function”, $x^{x^{\dots}}$. So the interpretation of f_k is the cumulative probability of shortness. The distribution with i_0 introductions follows $f_k^{i_0}$. As a worked example the chain-length probability depends on i_0 for a pathogen with $R_0 = 0.9$ according to:

```
# Iterated exponential
Ek = function(k, x) {
  out = rep(NA, k + 1)
  out[1] = 1
  for (i in 2:(k + 1)) {
    out[i] = x^(out[i - 1])
  }
  return(out)
}

# cumulative from single introduction
R0 = 0.9
fk = exp(-R0) * (Ek(20, exp(R0 * exp(-R0))) [-1])
i0 = 1
# uncumulate
g = c(fk[1]^i0, diff(fk^i0))
plot(g, ylab = "Probability", xlab = "Length", log = "y",
      pch = 16)
# loop from 1 to 10 introductions
for (i0 in 1:10) {
  g = c(fk[1]^i0, diff(fk^i0))
  lines(g)
}
points(g, pch = 17)
legend("topright", c("1", "10"), pch = 16:17)
```

With a single introduction the modal length is one, but with a fair chance of getting secondary and maybe tertiary cases. With five or 10 initial cases the modal chain length is three and seven, respectively. Obviously, a smaller R_0 leads to shorter typical chains of transmission.

For emerging pathogens with pericritical reproduction numbers above one, we sometimes see bimodal epidemic distributions with either minor clusters due to stochastic fadeout early on or major epidemics. Ebola is perhaps a good illustration with most of the several dozen reported outbreaks being small but two recent outbreaks in West Africa (2014-2015) and DRC (2016-2018) reaching into the thousands. Bailey (1957) and Bartlett (1960a) were among the first to study this bimodality from a theoretical point of view. This bimodality is also clearly seen in the predicted stochastic spread on social networks discussed in Sect. 14.6.

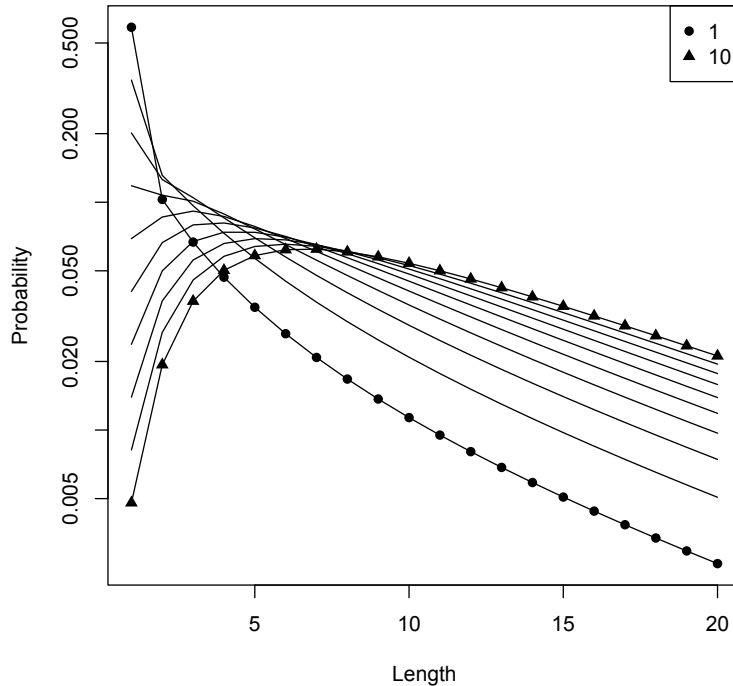


Fig. 15.2: Chain length distributions predicted from the Galton-Watson branching process assuming a Poisson distributed offspring distribution and subcritical spread with $R_0 = 0.9$ and size of initial introduction varying from one to 10

15.3 Phocine Distemper Virus

There are two particularly well documented stage IVa animal-to-animal supercritical spillovers of PDV from arctic harp seals (*Pagophilus groenlandicus*) to North Sea harbor seals (*Phoca vitulina*) and grey seals (*Halichoerus grypus*) in 1998 and 2002. Using the type of next-generation formalism of structured transmission discussed in Sects. 3.9 and 10.7, Klepac et al. (2009) estimated the reproduction number in harbor seals during the invasion to be in the 2–2.5 range. Like other morbilliviruses, PDV causes mortality or lifelong immunity in its hosts. Thus, like for measles, susceptible recruitment through birth is critical for sustaining chains of transmission.³ In prevaccination US and UK the measles critical community size was around 300–500k (Fig. 1.2; see also Bartlett, 1960b; Grenfell and Harwood,

³ Though there are Cetacean morbilliviruses documented from rare species of toothed whales which mode of persistence is not understood (van Bressen et al., 2014).

1997), which with a typical birth rate in these countries of around 20 births per thousand per year indicates that an annual recruitment of around 10k newborns is necessary to sustain local transmission. During 1920–40, New York city had a population size of around seven million people and birth cohorts of around 91k per year. London during the mid 20th century had a population size of three million and annual birth cohorts of 45k, so both cities were well above CCS recruitment levels. As a consequence both cities harbored violent sustained recurrent epidemics (Fig. 1.4).

Harbor seal communities (“haulouts”) in the Northeast Atlantic have numbers in the hundreds to several thousands (Special Committee on Seals, 2002), so pup production is way under the critical recruitment level for sustained transmission particularly due to the seasonal pulsing of reproduction (Swinton, 1998). The annual birth cohort of arctic harp seals, in contrast, is estimated to be around a million (Hammill et al., 2021) thus supporting the tenet that this represents the reservoir species for spillover to other seals.

Curiously the first reports of PDV in both were reported from the Danish island of Anholt in the Kattegat sea ($55^{\circ}20'N, 16^{\circ}10'E$) towards the inlet to the Baltic sea that is far away from the Arctic PDV reservoir. The pdv dataset holds the number of dead seals washed ashore across 25 Northern European areas during the 2002 epidemic starting in May and running through the end of the year (Harding et al., 2002). The chain of transmission ended in late 2002 due to the burnout of susceptibles. To visualize the invasion we can map the date of early numbers using cumulative strandings of > 20 as a benchmark (Fig. 15.3).

```
require(rworldmap)
# Day to 20 deaths
inv = apply(pdv$ts[, -1] < 20, 2, sum)
newmap = getMap(resolution = "low")
plot(newmap, xlim = c(-7, 16), ylim = c(50, 61), asp = 1.5)
# Big circles are early invasion. The ^1.5 is to
# increase contrast of early vs late invasion
invsymsize = (-inv - 275)/275)^1.5
symbols(pdv$coord$lon, pdv$coord$lat, circles = invsymsize,
        bg = gray(inv/275), inches = 0.15, add = TRUE)
```

Seals do not travel over land, so in terms of spatial spread of PDV some measure of seaway distance should be used. A quick search on rseek.org on converting a map into a “friction surface” can help identifying the paths of shortest seaway distance.⁴ The recipe requires several geospatial R packages:

```
require(raster)
require(gdistance)
require(maptools)
require(rgdal)
require(maps)
# the wrld_simpl data set is from maptools package
data(wrld_simpl)
```

⁴ Manipulation of geospatial data is an enormous field and the R community has generated a lot of resources beyond the scope of this text. The code is adopted from stackoverflow.com/questions/69258889.



Fig. 15.3: A depiction of the day of > 20 cumulated strandings of harbor seals across 25 locales in Northeastern Europe from early May 2002 through the end of that year. Large dark circles represents earliest invasion. The largest circle is the Danish island of Anholt

```
# make a default world projection
world_crs = crs(wrld_simpl)
world = wrld_simpl
worldshp = spTransform(world, world_crs)

# rasterize will set ocean to NA
ras = raster(nrow = 1000, ncol = 1000)
worldmask = rasterize(worldshp, ras)
worldras = is.na(worldmask)
```

```
# set land to very high friction
worldras[worldras == 0] <- 99
# create a friction object from the raster
tr = transition(worldras, function(x) 1/mean(x), 16)
tr = geoCorrection(tr, scl = FALSE)
```

The below code finds the shortest paths among the different seal haul-outs. This calculation is computationally quite expensive so the friction surface distances are included in the pdv data set of the epimdr2 package.

```
dmat99sc = matrix(NA, ncol = 25, nrow = 25)
par(mfrow = c(1, 2))
plot(A, xlim = c(-10, 20), ylim = c(45, 65))
for(i in 1:25){
  # function accCost uses the transition object
  # and point of origin
  port_origin = structure(as.numeric(pdv$coord[i, 3:2]),
    .Dim=1:2)
  port_origin = project(port_origin,
    crs(world_crs, asText = TRUE))
  A = accCost(tr, port_origin)
  for(k in i:25){
    port_destination= structure(as.numeric(pdv$coord[k,
      3:2]), .Dim=1:2)
    port_destination = project(port_destination,
      crs(world_crs, asText = TRUE))
    path = shortestPath(tr, port_origin, port_destination,
      output = "SpatialLines")
    t_path = shortestPath(tr, port_origin, port_destination)
    distance = costDistance(tr, port_origin, port_destination)
    lines(path, col = grey((i + 26)/56))
    dmat99sc[i, k] = dmat99sc[k, i] = distance[1, 1]
  }
}
plot(pdv$fs[1, ]/1000, as.vector(inv),
  xlab="Friction distance", ylab = "Day")
```

Figure 15.4a depicts the calculated shortest friction distances by sea between the haulouts and Fig. 15.4b shows days to > 20 dead seals against friction surface distance from Anholt. The strong positive relation to sea-way distance testifies to the spatially contagious nature of the spread of the virus. A similar pattern was seen during the 1988 epizootic (Swinton et al., 1998).

15.4 Rabies

The eastern US invasion of rabies in raccoons first discussed in Sect. 10.1 is particularly well documented in Connecticut because the cases were geolocated to individual townships. The first reports were from the southwestern corner of the state in March 1991. By January 1995 the virus had spread throughout the state. Smith et al.

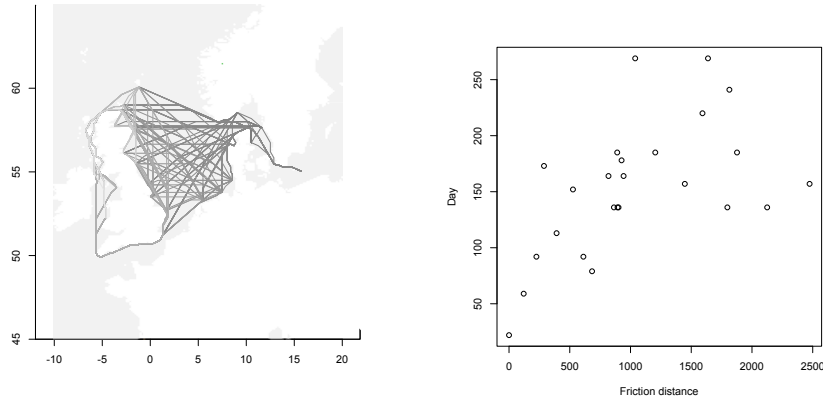


Fig. 15.4: (a) A depiction of the shortest sea distances between the 25 seal haul-outs that recorded significant die-offs during the 2002 PDV epizootic. (b) The day of report of > 20 dead seals against seaway friction surface distance from Anholt for each of the 25 well documented haulouts

(2002a) and Waller and Gotway (2004) provide a detailed statistical analysis of the spatial spread. The data that represents the month of first appearance for each of the 168 townships are in the `waller` data set.

```
data(waller)
head(waller)

##           x      y month
## 1 103.02200 68.71192    37
## 2 46.41953 28.43884    18
## 3 118.57160 88.25216    41
## 4 63.43697 76.50967    18
## 5 25.31975 91.60060    24
## 6 47.88734 35.93386    18
```

The `x` and `y` coordinates represent the geographic coordinates in kilometers from the southwestern corner. Following Waller and Gotway (2004) we can visualize the northeastward invasion of the virus (Fig. 15.5):

```
require(scatterplot3d)
s3d = scatterplot3d(waller$x, waller$y, waller$month,
  scale.y = 0.7, pch = 16, lwd = 2,
  color = gray(waller$month/max(waller$month)), type = "h",
  box = FALSE, xlab = "Easting", ylab = "Northing",
  zlab = "Month", angle = 120)
plane = lm(month ~ x + y, data = waller)
s3d$plane3d(plane)
```

Geolocated data on time-to-first-appearance (TFA) provides key information on rates and directions of spatial invasions of infectious diseases (Waller and Gotway,

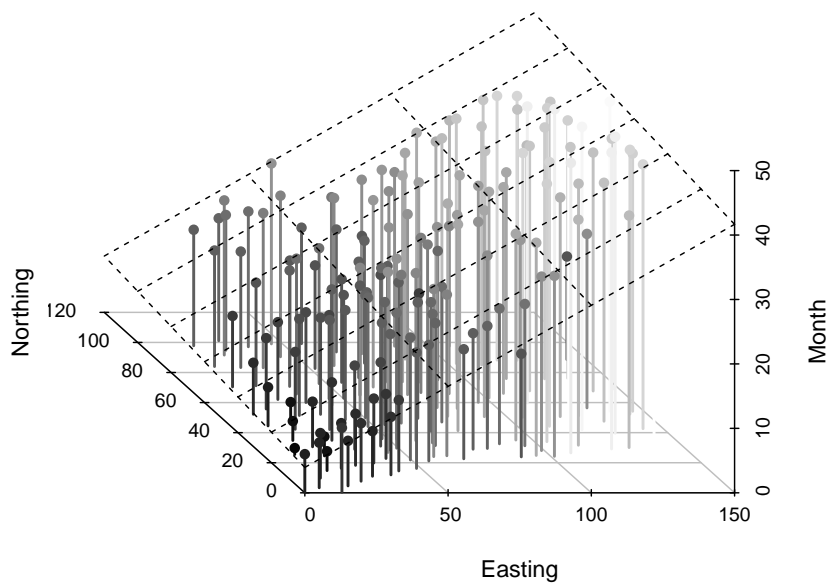


Fig. 15.5: Month of first report of raccoon rabies from March 1991 across 168 townships of Connecticut

2004) and other organisms of concern (Goldstein et al., 2019). A shallow smoothed surface of TFA across a landscape implies rapid range expansion, whereas slow spread result in a steep slope. If a spatial surface has a c_x slope in the x direction and a c_y slope in the y direction, then the steepest slope which reflect the spatial turnover is the geometric average of these and the invasion speed is the reciprocal. Thus, the speed of spread is $1/\sqrt{c_x^2 + c_y^2}$ and the dominant direction of spread (in radians) is $\arctan(c_y/c_x)$. For the raccoon rabies in Connecticut, the regression surface in Fig. 15.5 implies a speed of spread of about 4 km/month in a dominant 9° azimuth direction:

```
# speed
1/sqrt(plane$coef[2]^2 + plane$coef[3]^2)

##           x
## 3.927532

# direction
360 * atan2(plane$coef[3], plane$coef[2]) / (2 * pi)
```

```
##           Y
## 9.030879
```

In Eurasia the main host of rabies are the red fox. In Western and Central Europe a half century long enzootic of rabies started in the 1940s with a likely epicenter from Poland or Russia presumably as a spillover event from domestic dogs with subsequent spread throughout much of continental Europe. The virus was eventually eliminated⁵ from Western Europe in 2008 through an EU-wide concerted effort of air-deployed oral vaccine baits (Freuling et al., 2013).⁶ The European fox rabies enzootic have lead to many important disease ecological insights such as the notion of a critical host density (Anderson et al., 1981) discussed in Sects. 3.1 and 10.7. Further important issues showcase how mathematical models can be used to understand and predict speed of spatial diffusion of infectious disease across a landscape once nuances in host biology are considered (Murray et al., 1986; van den Bosch et al., 1990; Mollison, 1991). From the initial epicenter, fox rabies spread at around 30-60km / year. Appropriate models for spatial spread of infection depends on the nature of the spatial transmission process such as “distributed contacts” versus “distributed infecteds” (Reluga et al., 2006). For spread of human infections parallel notions are often coined as commuter spread versus migration spread (Keeling and Rohani, 2002; Keeling et al., 2004).

The notion of spatial kernels introduced in Sect. 12.2 is central to predicting spatial diffusion rates. The study by van den Bosch et al. (1990) assumed that rabies transmitted among foxes with relatively stable home ranges (and thus a distributed contact scenario) and derived an approximate formula for the expected wave speed of $c = u\sqrt{2\log R_0}/V$, where u is the standard deviation of the spatial transmission kernel (in this case related to the size of each home range) and V is the serial interval. With a serial interval of about 33 days and a typical home range size, van den Bosch et al. (1990) predicted a wave speed of 45 km per year at low densities and 30 km / year at high densities, as long as the fox density is above the critical host density (Anderson et al., 1981, Sect. 10.7) of around 1 fox per km^2 . Using a “distributed infecteds” scenario assuming foxes diffuse randomly across the landscape during the course of infection so u is related to the movement of foxes, Murray et al. (1986) predicted wave-like spread of rabies at a rate $c = u\sqrt{2(R_0 - 1)/V}$ (see also Mollison, 1991). With this calculation Murray et al. (1986) predicted a typical wave speed of around 50 km per year. In contrast to van den Bosch et al. (1990), the latter model predicts spread to increase with fox density. Mollison (1991) provides a discussion of different spread formulations, in general, and rabies and other case studies in particular.

⁵ Conventional usage is to use “eliminate” for regional control and “eradicate” for global control; Smallpox and Rinderpest are the only two viruses that have been eradicated through vaccination.

⁶ <https://tinyurl.com/msszkdjw> links to visualization of the invasion and elimination of fox rabies across Switzerland between 1967 and 1999.

15.5 Initial Control

The Spanish A/H1N1 influenza and SARS-CoV-2 pandemics are both exemplars of how overwhelmed hospital capacities lead to greatly exacerbated morbidity and mortality. For these, maxed out critical care units, respirators and medical staff led to greatly increased individual severity from infection. Sudden outbreak calamities with associated breakdowns of health infrastructure also had important indirect consequences as for example seen in the cessation of routine vaccination against important childhood diseases during the 2013-14 West African Ebola epidemic (Takahashi et al., 2015). These examples clearly illustrate that containing the height of an initial epidemic peak is very important for individual health and overall public health burden. The mantra during the early part of the SARS-CoV-2 pandemic was to “flatten the curve”. A vaccine is an obvious way to slow disease spread and other pharmaceutical interventions in the form of drugs may mitigate the stress on the health care system. In the absence of these, a number of non-pharmaceutical interventions (NPIs) were put in place in most countries.

As discussed throughout this text, the reproduction number is the transmission rate multiplied by the infectious period and for the closed epidemic (Sect. 3.1) the peak prevalence is $1 - (1 + \log R_0)/R_0$. Thus reducing the reproduction number will flatten the curve. It will also delay the timing of the peak (Bjørnstad et al., 2020a; Kröger et al., 2021) to allow for better preparedness. The various NPIs helped reduce the reproduction number in various ways; The transmission rate itself is the contact rate multiplied by the probability of infection given a contact, so social distancing reduce the rate and masking reduce the probability. Quarantining / self isolation decrease both the contact rate and stunts the effective infectious period because infected individuals are not mixing with susceptibles. There are analytic approximations to the time to peak incidence but they are quite elaborate (Kröger et al., 2021), so a shortcut is to do numerical analyses using the `sirmod` function introduced earlier. Figure 15.6 shows how peak prevalence and the time of the peak is predicted to depend on the reproduction number.

```
ip = tp = rep(NA, 201)
R0 = seq(1.2, 2.5, length = 201)
for (i in 1:201) {
  times = seq(0, 365, by = 0.01)
  paras = c(mu = 0, N = 1, R0 = R0[i], gamma = 1/7)
  paras["beta"] = paras["R0"] * (paras["gamma"] + paras["mu"])
  start = c(S = 0.99999, I = 1e-05, R = 0) * paras["N"]
  out = ode(y = start, times = times, func = sirmod,
             parms = paras)
  out = as.data.frame(out)
  ip[i] = with(as.list(paras), 1 - (1 + log(R0))/R0)
  tp[i] = out$time[which.min(abs(out$I - ip[i]))]
}
par(mfrow = c(1, 2))
plot(R0, ip, type = "l", xlab = "Reproduction number",
      ylab = "Peak prevalence")
plot(R0, tp, type = "l", xlab = "Reproduction number",
```

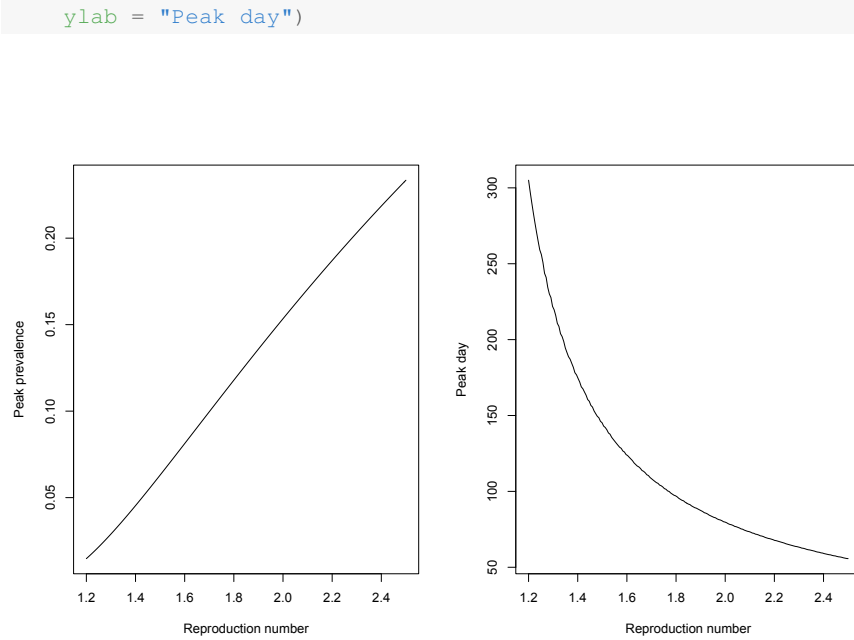


Fig. 15.6: The predicted (a) peak prevalence and (b) day of the peak as a function of the reproduction number assuming an infectious period of 7 days with a single initial infectious individual in a 100k population

Bjørnstad et al. (2020a) provides an interactive online shinyApp to do scenario analysis of NPI reduced reproduction numbers, peak and time-of-peak prevalence.

15.6 Synchrony

Elimination—the local control of infectious disease—is generally a matter of locally deploying pharmaceutical and non-pharmaceutical interventions sufficiently to push the reproduction number below one and thus break the chain of transmission. Eradication, in contrast, is a conceptually and practically tougher problem because it involves simultaneously breaking the chains everywhere. Section 1.3 visited on the notion that pathogens can persist regionally in host-pathogen metapopulations even if chains break during post-epidemic troughs (Grenfell and Harwood, 1997). As has been studied in great detail in general ecology, robust metapopulation persistence depends on spatial asynchrony among the coupled local populations (Hanski, 1998). With a high degree of synchrony, troughs will be aligned and there will be little opportunity for spatial rescue effects for a pathogen to evade eradication. Keeling et al. (2004) review how there is a tight interdependence between spatial coupling,

synchrony and regional persistence. It turns out all three may be strongly affected by vaccination. We can visit on this using the historical data from measles across England and Wales.

Grenfell and Harwood (1997) and Lau et al. (2020) outlined using measles as the exemplar the difference between source-sink metapopulations, locally coupled metapopulations and globally coupled metapopulations. In the latter setting the coupling can either be spatially structured or spatially random. The CMLs discussed in Sects. 12.6 and 12.10 are examples of models of local coupling. The gravity model discussed in Sect. 12.9 is a spatially structured, globally coupled formulation. Pre-vaccination measles was a source-sink metapopulation in which for England and Wales some 5–10 large cities above the critical community size (Fig. 1.2) sustained chains of transmission through the troughs to fuel recurrent hierarchical waves of reintroduction to smaller communities (Grenfell et al., 2001). The m4494 dataset has the case counts and locations for each of 354 locations (cities and villages) that has been collated in a geographic fashion such that it represents spatially consistent time series for each week from 1944 through 1994 (Lau et al., 2020). We can use the nonparametric spatial covariance function discussed in Chap. 13 to study patterns of spatial synchrony in 1950–60 pre- and 1980–89, 1990–94 vaccination periods.

```
require(ncf)
data(m4494)
pre = m4494$year >= 50 & m4494$year < 60
post = m4494$year >= 80 & m4494$year < 90
late = m4494$year > 90
s5059 = Sncf(x = m4494$longlat[, 1], y = m4494$longlat[, 2], z = m4494$measles[, pre], latlon = TRUE)
s8089 = Sncf(x = m4494$longlat[, 1], y = m4494$longlat[, 2], z = m4494$measles[, post], latlon = TRUE)
s90 = Sncf(x = m4494$longlat[, 1], y = m4494$longlat[, 2], z = m4494$measles[, late], latlon = TRUE)
plot(s5059, ylim = c(-0.1, 0.6))
plot(s8089, add = TRUE)
plot(s90, add = TRUE)
legend("topright", c("50-59", "80-89", "90+"), lty = 1, lwd = 3, col = c(gray(0.6), gray(0.8), gray(0.8)))
```

The covariance functions reveal local synchrony that decays with distance testifying to a dominance of local coupling particularly in the prevaccination period (Fig. 15.7). The local and hierarchical coupling is responsible for the gravity-like spread (Xia et al., 2004; Lau et al., 2020) discussed in Sect. 12.9 and recurrent spatial outbreak waves from large cities to surrounding conurbations (Grenfell et al., 2001). The relatively high region-wide average correlation of 0.25 (CI: {0.23, 0.27}) is partially due to the shared term-time forcing due to the yearly cycle of opening and closing of schools. The 1980–1989 period, which had an average vaccine cover of 73%, also exhibit evidence of distance decay and local coupling with a region-wide correlation of 0.14 (CI: {0.13, 0.15}). In contrast, the epidemics during the 1990–94 period are completely decorrelated (correlation: 0.02) despite recording 56,765 cases during the period. In an elaborate statistical analysis, Lau et al. (2020)

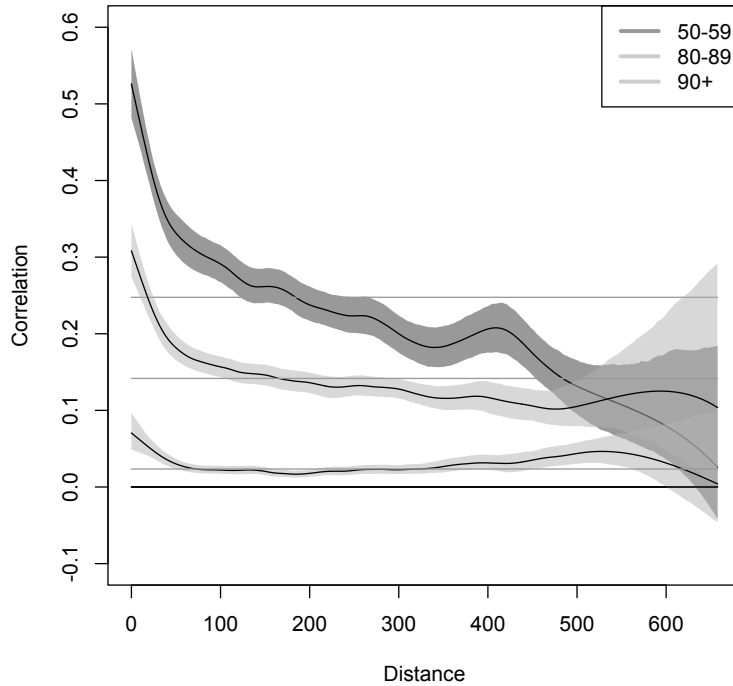


Fig. 15.7: The nonparametric spatial covariance functions of measles synchrony against separating distance for the 354 cities and villages in England and Wales in the 1950–59 prevaccine, 1980–89 early vaccine (mean cover: 71%) and the 90–94 late vaccine period (91% cover)

showed that the decorrelation is associated with a transition in the geometry of spatial coupling in the measles metapopulation. Whereas the probabilistic spread during the prevaccination era seems to adhere relatively well to predictions of the gravity model, this gave increasingly way to spatially random seeding of local epidemics as vaccine cover increased.

15.7 Coupling

Despite frequent local pathogen extinction, persistence may occur if there is spatial contagion among communities that exhibits asynchronous outbreaks. Thus, coupling and synchrony are key properties when it comes to the feasibility of eradication.

tion. The next section (Sect. 15.8) will attempt a more comprehensive synthesis pertaining to metapopulation persistense and eradication, but first consider these two factors. Intuition suggests that coupling is a two-edged sword: Too little spatial contagion will result in too infrequent recolonization and regional extinction, but too much may result in geographic homogenization and loss of asynchrony, alignment of troughs and regional extinction. Keeling et al. (2004) studied a spatially extended stochastic model of whooping cough to verify the idea of enhanced persistence at intermediate levels. We can revisit this analysis using a simple spatially extended TSIR model using the transmission parameters estimated for New York measles in Sect. 11.2. The New York case study is useful because its chaotic dynamics are prone to extinction during the deep post-epidemic troughs unless communities are very large (like New York which grew from 5.6M to 7.5M between 1920 and 1940).

```
# TSIR transmission coefficients
btny = c(32.552, 36.048, 43.163, 36.072, 37.459, 36.692,
       32.089, 35.116, 37.03, 29.915, 28.114, 20.413, 18.03,
       17.027, 15.855, 15.85, 18.87, 21.152, 26.08, 35.359,
       35.859, 34.128, 37.66, 34.19, 27.827, 38.87)
```

For simplicity the below assumes a metapopulation with p identical patches⁷ that are globally coupled with strength c in a commuter fashion. Thus, if the local force of infection in community i at time t is $\phi_{i,t} = \beta_{i,t}I_{i,t}$, it will exert a pressure $(1 - cp)\phi_{i,t}$ on the local susceptibles and contribute additional $c\phi_{i,t}$ to the force of infection in each of the other communities. In addition to parameters p and c , the `tsirSpat` function takes the same parameters as the `tsirSim2` function from Sect. 8.6 except the list of initial conditions needs to contain two vectors of length p representing initial susceptibles and infecteds for each patch.

```
tsirSpat = function(beta, alpha, B, N, p, c, inits, type = "det"){
  type = charmatch(type, c("det", "stoc"), nomatch = NA)
  if(is.na(type))
    stop("method should be \"det\", \"stoc\"")
  IT = dim(B)[1]
  s = length(beta)
  lambda = matrix(NA, nrow = IT, ncol = p)
  I = matrix(NA, nrow = IT, ncol = p)
  S = matrix(NA, nrow = IT, ncol = p)

  I[, 1] = inits[[1]]
  lambda[, 1] = inits[[2]]
  S[, 1] = inits$Snull
  cmat = matrix(c, ncol = p, nrow = p)
  diag(cmat) = 1 - c * p
  for(i in 2:IT) {
    lambda = beta[((i - 2) %% s) + 1]*cmat %*% (I[i - 1, ]^alpha)*S[i - 1, ]/N
    if(type == 2) {
      I[, i] = rpois(p, lambda)
    }
    if(type == 1) {
```

⁷ The code is actually vectorized so can accommodate N as a vector of varying population sizes.

```

        I[i, ] = lambda
    }
    S[i, ] = S[i - 1, ] + B[i, ] - I[i, ]
}
return(list(I = I, S = S))
}

```

As an illustration assume five patches and draw initial conditions from the log-susceptible time series (`lS0ld`) and corrected infected time series (`Ic`) from Sect. 11.2.⁸ The first run is assuming no spatial coupling and a simulation for 100 years:

```

p = 5
pinits = list(Snull = sample(exp(lS0ld), size = p),
               Inull = sample(Ic, size=p))
sim2 = tsirSpat(beta = btny, alpha = 0.98,
                 B = matrix(median(NY$rec), ncol = p, nrow = 2600),
                 N = median(N), p = p, c = 0, inits = pinits, type = "stoc")
mean(cor(sim2$I)[upper.tri(cor(sim2$I))])

## [1] NA

matplot(sim2$I, type="l", log="y", xlim=c(0,400),
         col = 1, xlab = "biweek", ylab = "I")

```

In the particular stochastic realization shown in Fig. 15.8 chains of transmission were all broken by about 10 years (260 biweeks). Armed with this general simulator one can study how spatial coupling affects local/global extinction rates and synchrony in the five patch system. The below looks at 100 stochastic realizations across a range of spatial contagion rates:

```

#coupling
coup = seq(0, 0.025, by = 0.0005)

sync = gext = lext = matrix(NA, ncol = length(coup), nrow = 100)
for(k in 1:length(coup)){
  for(j in 1:100){
    sim2 = tsirSpat(beta = btny, alpha = 0.98,
                     B = matrix(median(NY$rec), ncol = p, nrow = 2600),
                     N = median(N), p = p, c = coup[k], inits = list(Snull =
                           sample(exp(lS0ld), size = p),
                           Inull = sample(Ic, size = p)), type = "stoc")
    #global extinction time
    gext[j, k] = 2600 - sum(apply(sim2$I, 1, sum) == 0)
    #fraction of local absence before extinction
    lext[j, k] = sum(sim2$I[1:gext[j, k], ] == 0) / (gext[j, k] * p)
    #synchrony
    sync[j, k] = mean(cor(sim2$I)[upper.tri(cor(sim2$I))])
  }
}

```

⁸ So for this code to work the previous susceptible reconstruction must be available).

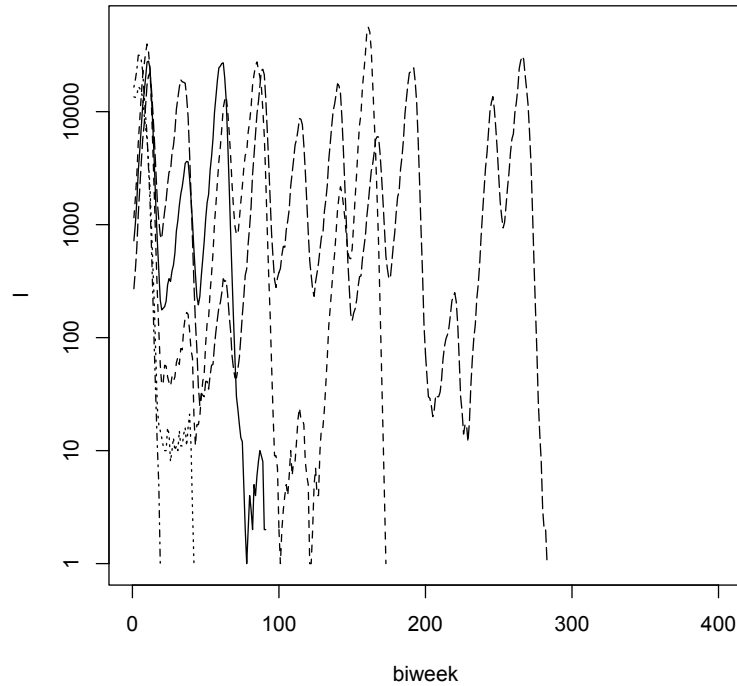


Fig. 15.8: A stochastic realization of the five patch spatial TSIR model assuming prevaccination New York transmission patterns and no spatial coupling. All chains of transmission broke within the first 5–10 years

The results (Fig. 15.9) verify the intuition. With low spatial contagion there is very little synchrony because of the underlying unstable dynamics and local extinction—here defined as the fraction of time of local absences among the communities while the pathogen is still circulating within the metapopulation—is frequent because spatial rescue is infrequent (Fig. 15.9a). As a consequence, the time to global extinction is short despite the substantial asynchrony (Fig. 15.9b). With strong coupling, time to global burn-out is short and local extinction is relatively high because the spatial contagion leads to synchronization. There is a goldilocks zone for which most stochastic realizations predict regional persistence past the 100 year horizon (Fig. 15.9b).

```
boxplot(sync, outline = FALSE, xaxt = "n", xlab = "coupling",
        ylim = c(0, 1))
boxplot(lext, col = 0, outline = FALSE, , xaxt = "n",
        add = TRUE)
```

```

legend("right", c("Synchrony", "Local \n extinction"),
       pch = 22, pt.cex = 2, pt.bg = c("gray", 0), bty = "n")
boxplot(gext/26, xaxt = "n", xlab = "coupling")
legend("topright", c("Extinction\n time (yrs)"), pch = 22,
       pt.cex = 2, pt.bg = c("gray"), bty = "n")

```

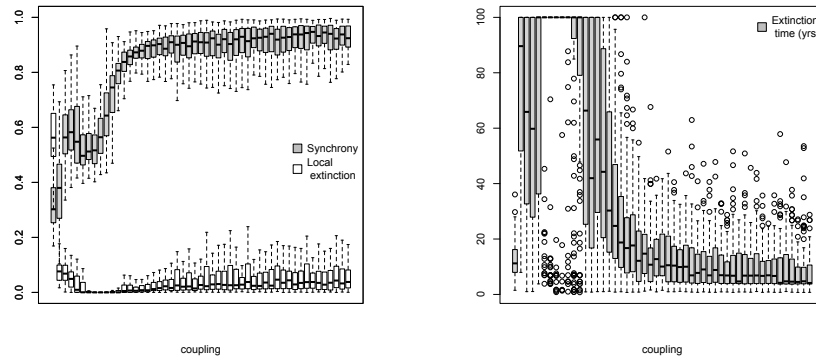


Fig. 15.9: (a) Boxplots of synchrony and local rates of extinction. Local rates of extinction is, here, defined as the fraction of time of local absences while the pathogen is still circulating within the metapopulation. (b) time to global extinction as a function of coupling strength in the five patch metapopulation model. Open circles represents outlying outcomes among the simulations

15.8 A Synthesis

Eradication equates to regionalized metapopulation non-persistence. As alluded to in the previous sections forces influencing metapopulation persistence are multitude and are affected by both local and spatial processes. In the balance are local extinction, recolonization, coupling and asynchrony. As a wrap-up of the main part of this monograph, the nuances and complexities are attempted summarized in Fig. 15.10.

Increased coupling ② will—all else being equal—enhance persistence because it leads to rescue from local breaks of chains of transmission (Metcalf et al., 2013). As highlighted above, this area has been explored in great depth in the general field of ecology (Hanski, 1998; Hanski and Gaggiotti, 2004). However, coupling in epidemic metapopulations also ① lead to loss of asynchrony and thus ④ reduce regional persistence as detailed in Sect. 15.7 and illustrated in Fig. 15.9 because of resultant diminished rescue effects.

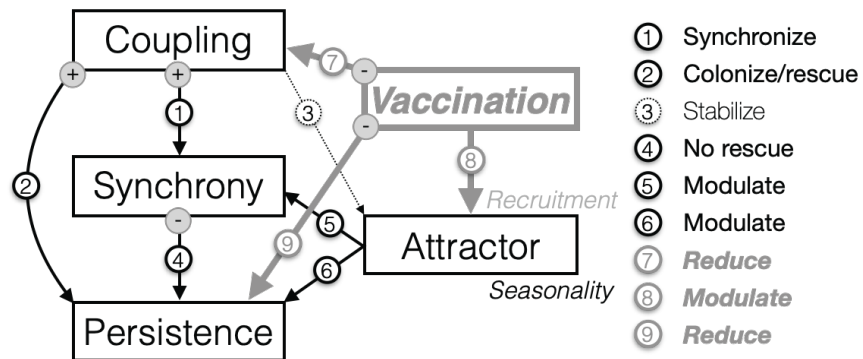


Fig. 15.10: A synthetic chart of some processes governing regional persistence as influenced by mass vaccination

Chapters 6 and 11 discussed the notion of attractors to characterize disease dynamics across a spectrum from stable endemicity, annual or multi-annual cycles to chaotic fluctuations. It turns out the nature of the attractor influences regional persistence in two separate but important ways. When seasonality is strong enough to push dynamics into the erratic regime, ⑥ post-epidemic troughs tend to be very deep veering into the Atto-fox territory of (Mollison, 1991) leading to broken chains of transmission and reduced persistence (Ferrari et al., 2008). Though, as illustrated in Fig. 15.9 the associated asynchrony may prop up persistence. More curious ⑤ is the phenomenon of nonlinear phase-locking. The propensity for synchronization is sensitively dependent on the nature of the attractor (Bjørnstad et al., 1999b; Bjørnstad, 2000). Chaotic dynamics is usually hard to synchronize (Ruxton, 1994) and may therefore contribute to disease persistence. Stochastic, but asymptotically stable endemic, will generally inherit synchrony according to the strength of spatial coupling (Kendall et al., 2000). Local limit cycles, in contrast “yearn to synchronize” (Bjørnstad et al., 1999b; Bjørnstad, 2000) through the process of nonlinear phase-locking.⁹ With low seasonality dynamics are asymptotically stable and synchrony is governed by coupling. With high seasonality the dynamics is erratic (Fig. 15.11b) but synchrony is comparable. In contrast, with intermediate seasonality which result in biennial cycles (Fig. 15.11b), spatial synchrony is almost perfect (Fig. 15.11a) due to the nonlinear phase-locking. Bjørnstad et al. (1999b) discuss this in general. Rohani et al. (1999) and (Bjørnstad, 2000) provides evidence that this is a true phenomenon in infectious disease dynamics. Rohani et al. (1999) showed that vaccination resulted in different changes in synchrony for whooping cough and measles. For whooping cough synchrony increased while for measles it decreased. For measles this was associated with vaccine-induced loss of cyclicity as per discussion in Sect.

⁹ As described by watchmakers centuries ago who noted how clocks hanging on a common wall would lock-step.

6.6. For whooping cough Rohani et al. (2002) argued that the gain of cyclicity was due to the presence of the multiannual almost attractor discussed in Sect. 11.5.

We can use the spatial TSIR model to investigate the relation between attractor type and propensity for synchronization. As discussed in Chap. 6, increasing seasonality pushes dynamics from annual, to cyclic multiannual and to erratic epidemics. The following code simulates a 10-patch TSIR model assuming a coupling $c = 0.001$ and with varying degrees of seasonality for a 30 year time frame. The among-patch synchrony is assessed from the last 20 years of the simulation (Fig. 15.11a).

```

#Fig A
mbtny = mean(btny) #mean beta
p = 10 #number of patches
seasseq = seq(0, 0.3, by = 0.01) #seasonality
sync = gext = lext = matrix(NA, ncol = length(sdseq), nrow = 500)

for(k in 1:length(seasseq)) {#loop over seasonality
  for(j in 1:500) { #500 times
    bnty = exp(scale(log(btny)) * seasseq[k] + log(mbtny))
    sim2 = tsirSpat(beta = bnty, alpha = 0.98,
                     B = matrix(median(NY$rec), ncol = p, nrow = 780),
                     N = median(N), p = p, c = 0.001, inits =
                     list(Snull = sample(exp(lSold), size = p), Inull =
                     sample(Ic, size = p)), type = "stoc")
    gext[j, k] = 780 - sum(apply(sim2$I, 1, sum) == 0)
    lext[j, k] = sum(sim2$I[1:gext[j, k], ] ==
                     0) / (gext[j, k] * p)
    #synchrony during year 10-30
    sync[j, k] = mean(cor(sim2$I[261:780, ]) [upper.tri(
      cor(sim2$I[261:780, ]))])
  }
}
boxplot(sync, outline = FALSE, xaxt = "n", xlab = "Seasonality",
        ylab = "Synchrony")

```

In addition to charting the level of synchrony, it is instructive to plot annual stroboscopic sections as a bifurcation diagram (Fig. 15.11b). Because the TSIR is stochastic, the bifurcation lines are fuzzy, however the transition from annual, biennial and chaotic regimes are clear. The annual regime is associated with synchrony rising from 0.2. The chaotic regime is associated with synchrony of 0.4–0.5 because of increased shared seasonality. The biennial cycles are generally almost perfectly aligned despite the modest spatial coupling—The phenomenon of non-linear phase-locking.

```

nrow = 52000 - 20), N = median(N), p = p, c=0.001,
inits = list(Snull = sample(exp(lSold), size = p),
Inull = sample(Ic, size = p)), type = "stoc")
points(rep(seasseq[k], 2000 - 20), sim2$I[seq(from = 521,
to = 52000, by = 26)], pch = 20, cex = 0.3)
}

```

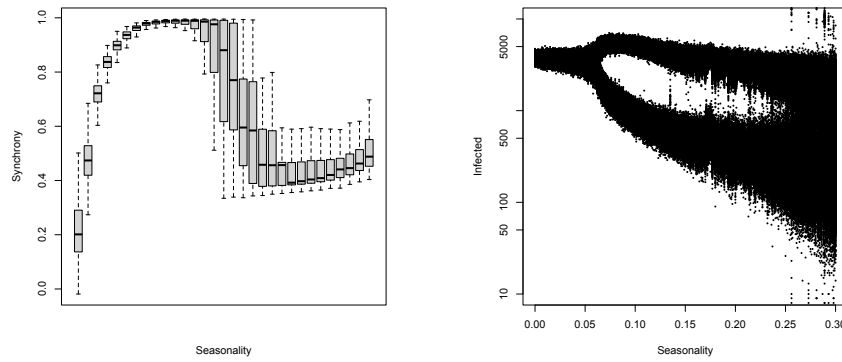


Fig. 15.11: (a) Synchrony versus seasonality. (b) Annual stroboscopic bifurcation diagram against seasonality

When it comes to introductions of mass-vaccination campaigns, there is an important notion of a honeymoon period during which diseases are seemingly fully controlled due to the background of substantial infection-induced immunity (Scherer and McLean, 2002; Klepac et al., 2013) after which substantial flare-ups may happen due to creeping buildup of susceptibility due to absence of circulation (Graham et al., 2019, 9.8). The metapopulation perspective adds to this by suggesting that in the aftermath of vaccine rollout there may be a period of infrequent spatial pathogen spread because of previous spatial epidemic synchrony. The subsequent change in spatial dynamics may over time give rise to more robust metapopulation persistence with increasing vaccine-induced asynchrony. Vaccination, thus, affects spatiotemporal dynamics in multiple ways. First, ⑦ it decreases spatial coupling because with lower numbers of susceptibles and infecteds there is less opportunity for spatial contagion. Second, ⑧ because it modulates dynamics towards greater or weaker cyclicity it affects levels of synchrony and thus propensity for regional persistence. Finally, ⑨ vaccination generally reduces persistence because of the more frequent breaks in chains of transmission.